Modelling plastic heating and melting in a semi-batch pyrolysis reactor

Shawki Mazloum, Sary Awad, Nadine Allam, Youssef Aboumsallem, Khaled Loubar, Mohand Tazerout

Modelling plastic heating and melting in a semi-batch pyrolysis reactor.

Shawki MAZLOUM[1,2], Sary AWAD[1], Nadine ALLAM[2], Youssef ABOUMSALLEM[2], Khaled LOUBAR[1], Mohand TAZEROUT[1]

[1] *GEPEA, UMR 6144, Energy Systems and Environment Department, IMT Atlantique, 04 rue Alfred Kastler, CS 20722, 44307 Nantes Cedex 3, France.*

[2] *Lebanese International University, Beirut, Lebanon*

**Corresponding author:* Sary AWAD, *sary.awad@gmail.com*

Abstract

Plastic pyrolysis is a solution for the dilemma of enormous plastic waste accumulation and an alternative source of energy, which converts plastic wastes into a wide range of fuels and chemicals by thermal decomposition. The concept is widely validated and applied at lab-scale in terms of characterisation of the process and its by-products. On the other hand, numerical modelling and optimizing of the process for the sake of developing and efficient implementation at the industrial scale are seldom reported in literature. And since there exist different phenomena involved during this process (starting from feeding with raw material until the recovery of products), the aim of this work is to model and validate heating and melting phenomena of plastics, using finite element method, inside a semi-batch reactor as a first step preceding the cracking phenomenon. First, sensible heat transfer within the reactor, empty or loaded with solid and liquid materials, is modelled by coupling the energy and the momentum equations, where the results are validated experimentally at different heating rates. Moreover, a modified apparent heat capacity method (AHCM) is used to model the melting phenomena of plastics, which revealed good capability. As a result, the model is validated through temperature profiles measured at different points on the semi-batch reactor and by addressing energy balance on the whole experiment. Whereas, the average relative error between experimental and simulated results, at different heating rates didn't exceed 8%. Finally, the validated model has paved the way for modelling the whole pyrolysis process of plastics.

Keywords: polypropylene; simulation; finite elements; melting; AHCM method

1. Introduction

Since the beginning, plastic materials were presented as an arrangement to substitute the rare and non-sustainable assets such as tortoiseshell, ivory and animal bones. Since at that point, plastics have shaped the world and they are involved in our everyday life bringing security, hygiene,

consolation and prosperity to our society. Since 1950s, the world's annual plastic production has increased from 1.7 million tons into nearly 360 million tons in 2018; around 18% were produced in Europe and more than 50% in Asia [1]. At the end of its service life, varying from one day to more than 50 years, plastics form solid wastes. Therefore, due to the huge annual plastic production and its short life span, plastic wastes production reached 307 million tons worldwide in 2015, where 60% are polyolefin materials i.e. polyethylene (PE) and polypropylene (PP) [1], and the rate is still increasing [2]. Depending on their physical and chemical characteristics, the collected plastic wastes can be sent to mechanical reprocessing, to feedstock / chemical re-cycling handle or to energy recovery or landfilling. In Europe, 29.1 million tons of plastic post-consumer wastes were collected and treated in 2018; 32.5% are recycled, 42.6% are used for energy recovery and 24.9% are landfilled [1]. Whereas, landfilling is not an environmental process due to the fact that plastic materials are non-biodegradable. Therefore, the dilemma of the enormous plastic wastes production and land and water pollution, that it caused are still not solved. On the other hand, in order to achieve plastic circular economy and to reduce the plastic wastes pollution, landfilling treatment should be decreased, whereas recycling and recovery processes must be more employed [1]. But due to the limitation of recycling process and its high cost and intensive labor, energy recovery processes are more preferable. Moreover, plastic pyrolysis is one of the most efficient and green energy recovery processes; It converts plastic wastes into fuel by heating it in absence of oxygen, thus avoiding incineration and toxic gases emission [3]. Therefore, plastic pyrolysis process is a convenient and environmental solution for plastic wastes accumulation, which needs to be conceived and widely applied at the industrial scale. On the other hand, many studies focused on pyrolysis kinetics [4, 5], operating parameters [6] and characteristics of by-products at a lab-scale [7]. Whereas, numerical modelling and optimizing of the process for the sake of developing and efficient implementation at the industrial scale are seldom reported literature.

Bockhorn et al. [8] and Navarro et al. [9] numerically simulated pyrolysis for plastic particles to determine the kinetic parameters from the thermogravimetric analyser data. The global heat transfer coefficient used was related to different reactor configurations: 10 $W.m^{-2}.K^{-1}$ for fixed bed rectors, while a range between100 $W.m^{-2}.K^{-1}$ to 1000 $W.m^{-2}.K^{-1}$ is typical for fluidized-bed reactors [9]. Whereas, Jin et al. [10] modelled pyrolysis process for polyethylene (PE), polypropylene (PP), and polystyrene (PS) in a vertical falling film reactor, using the volume of fluids (VOF) model, in order to track the gas-liquid interface of the two-phase flow [11-13]. Moreover, they mentioned that the apparent heat transfer coefficient of molten plastic in falling film reactor is about 4000 $W.m^{-2}.K^{-1}$ and is greater than that observed in rotary kiln reactor, which is about 1000 $W.m^{-2}.K^{-1}$ [14]. Furthermore, Csukas et al. [15] modelled plastic pyrolysis in a continuous tubular reactor using Direct Computer Mapping (DCM), but they didn't calculate the overall heat transfer coefficient. For the reaction model, the one-step model is used by many researchers and revealed consistency in describing plastic pyrolysis [16, 17]. Ding et al. [16] used the one-step model to model pyrolysis for plastic particles inside a fluidized bed reactor; the results of the method were validated experimentally.

Nevertheless, all mentioned studies used semi-empirical models and overall heat transfer coefficients to model the process. The flaw of semi-empirical approaches is that they are

dependant of operating conditions and experimental set-ups and are rarely extendible to more general cases. It is noticed that literature about pyrolysis is missing models based on the solution of governing equations (energy equation, heat transfer, mass transfer and momentum equations) using finite element approach. In addition, modelling and optimizing efficient plastic pyrolysis reactors that would be applied and invested at the industrial scale is not done yet. Therefore, in order to achieve an overall design and conception of an industrial plastic pyrolysis reactor, pyrolysis process is recommended to be modelled and validated at a lab-scale as a first step, due to the complexity of such procedure. Then this model is upgraded and numerically optimized (geometry, process, boundary conditions, etc.) to be later on built and checked experimentally. Moreover, the knowledge of Computational Fluid Dynamics (CFD) represents a vital aspect in accurately modelling and simulating such complex processes. CFD is said to be the science that predicts fluid flow using computational methods and algorithms (module) to solve the mathematical equations that govern the fluid flow. Therefore, understanding the current fluid motion and choosing the appropriate mathematical models and parameters are the first steps in modelling any fluid flow problem. Fluid flow regimes may be represented by single-phase or multiphase flows, laminar or turbulent flows, free or porous media flows, and compressible or incompressible flows. Moreover, within each type of flow there exist further different complex models and details that expand to apprehend the nature of the existing fluid flow. For example, various closure models for turbulent flows such as k-ε model, k-ω model, SST model, algebraic yPlus model, etc… In addition, CFD module can be coupled with heat transfer and chemical reaction modules (governing mathematical equations) to model more complex real life processes [18, 19].

Depending on what preceded and knowing the fact that plastic pyrolysis process passes through different sub-processes, like heating and melting, before undergoing thermal cracking, , this paper forms a first step in modelling and validating plastic pyrolysis process at lab-scale level. The objective of this work is to model plastic heating and melting processes in a semi-batch reactor using COMSOL Multiphysics software and to validate the model using experimental data. Many researchers investigated melting process and heat convection for specific materials, other than plastic, that can help us in modelling the plastic melting process. Madruga et al. [20] made experimental investigation and numerical study on melting tetracosane paraffin within a cubic enclosure. The initial temperature of tetracosane was set at 40 °C and heated from the bottom that was held at 80 °C. Therefore, the thermal diffusivity is low and the tetracosane is heated and melted slowly by a uniform surface temperature. Moreover, Madruga et al. used the apparent heat capacity method (AHCM) to model melting process of tetracosane, but they used a linear function to describe the phase transition. The numerical and experimental results were in a good agreement. In addition, Samara et al. [21] and Murray et al. [22] also used AHCM to model the melting process of phase change material (RT25) and octadecane respectively. Again the used phase change materials have a low melting temperature (T_m = 27 °C) and are heated using a uniform heat flux. In contrast, Salvi et al. [23] mentioned the AHCM in their work, where they modelled the phase change for carboxymethyl cellulose solution by microwave heating, but they used a predefined Gaussian distribution function (δ) to model the latent heat during phase change. The average numerical values of temperature were in fairly good agreement with the average experimental temperatures for carboxymethyl cellulose (R^2 = 0.91).

On the other hand, modelling and validating plastic heating and melting at high temperatures inside a batch reactor or a fixed enclosure is rarely reported in literature. Consequently, in our case the semi-batch reactor is heated by electrical heating coils with high heating rates (10 – 20 °C/min), and non-uniform temperatures. Moreover, the reactor is heated from ambient temperature up to temperatures that could reach 570 °C for a large interval of time, which adds more difficulties for validation. Also, a simulated controller is employed to mimic the role of the experimental heating coils.

In order to take in considerations all aforementioned difficulties, the modelling work was led at four consecutive steps, adding more challenges at each new one. The first step considered was to simulate the heat transfer within the empty reactor in order to calibrate its materials properties and to adjust the related assumptions. On the second, third and fourth steps the sensible and latent heat transfer phenomena by conduction and convection were decoupled by studying each one at a part. Thus sand, vegetable oil and ice were chosen for sensible heat transfer by conduction, sensible heat transfer by convection and latent heat transfer phenomena, respectively. For experiments dealing with fluids the energy equation (heat transfer module) was coupled to the momentum equation (Navier-Stokes Equations) using temperature dependency material properties and a body force to model the natural heat convection of a single-phase laminar fluid flow inside the reactor. Furthermore, the AHCM with a smooth Heaviside transition function is used to model plastic melting process, which is not yet referred in literature.

2. Experimental setup

2.1. Laboratory scale pyrolysis reactor

The semi-batch reactor shown in Fig. 1 is a stainless steel hollow cylinder of 200 mm height, 80 mm inner diameter, and 4 mm thickness. The reactor is heated by a 1500 W electrical coil coupled to a programmable controller that regulates final temperature. The power consumed by the electrical heater is measured and recorded. A ceramic fibre jacket covers the reactor for thermal insulation. The reactor is equipped with five K-type thermocouples (diameter: 0.1 mm, uncertainty: ±0.1 K) to measure the temperature at different locations as shown in Fig. 1 (a). The reactor temperature is controlled via wall temperature T_2. Moreover, thermocouple T_1 is plunged inside the reactor to monitor the feedstock temperature. Earlier to heating, the reactor is purged with Nitrogen gas (N_2) for 15 min to guarantee an inert environment.

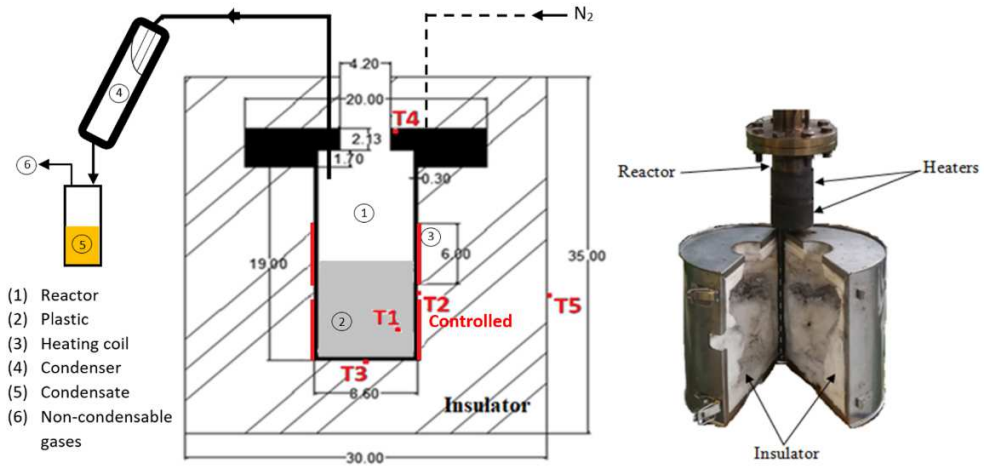

Fig. 1. Schematic diagram, units are in cm, (a) and real image of the semi-batch reactor (b).

2.2. Experiments

Three series of experiments are realized at different heating rates (10, 20 and 30 % of the heater full load 1500 W) and each experiment is done at least in two replicates. In each experiment, temperatures at different positions are recorded to be compared later to the simulated results. The heating rates are chosen depending on the type of pyrolysis that will be led later in the semi-batch reactor, which is supposed to be slow pyrolysis with heating rates below 10 °C/min. Moreover, first series of experiments were heating blank reactor to 490 °C at different heating rates then cooling it. Whereas, the second series of experiments were heating reactor filled with sand to 570 °C at different heating rates. As for the third, the reactor was filled with light viscous fluid, sunflower oil, and heated with different heating rates to reach 180 °C. The viscosity of the sunflower oil was measured at different temperatures using AND vibro viscometer and results are shown in Table 1. The viscosity drops logarithmically from 51 mPa.s at ambient temperature (25 °C) to 3.3 mPa.s at 180 °C.

Table 1
Dynamic viscosity of sunflower oil

Temperature (°C)	**25**	**30**	**40**	**50**	**60**	**70**	**80**	**90**	**110**	**120**	**140**	**160**	**180**
Viscosity (mPa.s)	51	42	29.2	21.1	15.9	12.2	9.6	7.7	6.3	5.7	4.7	3.9	3.3

Finally, the last series were phase change experiments: melting ice and melting PP. The plastic samples used in melting and pyrolysis are granular virgin polypropylene with particle size of, approximately, 2 – 3 mm. In order to avoid porosity issues inside reactor, before each experiment, the loaded PP particles were melted then cooled to ambient temperature to have a

bulk of solid plastic inside the reactor. SETSYS Evolution TGA-DTA / DSC instrument was used to evaluate melting and heating of PP at different heating rates varying between 5 and 10°C/min. The determined range of melting specific enthalpy is 60-65 kJ/kg.

2.3. Materials and methods

The reactor is modelled as 2D-axisymetric, because of its symmetrical shape, to reduce the computational time. In addition, the numerical studies for all of the experiments were carried out using COMSOL Multiphysics software. All of the corresponding simulations were converged with an absolute tolerance of 0.0001. The fully coupled approach was used for the numerical calculation instead of the segregated approach, where all the dependent variables (T, and $\vec{\mathbf{v}}$) were evaluated at the same time and not subsequently. Moreover, the PARDISO (Parallel Direct Solver) algorithm, which is based on lower-upper decomposition method for matrices, was used along with the Newton's Method (Newton-Raphson Method), with automatic damping factor, to calculate the solution at each time step taken by the solver. Consequently, the time stepping method follows the BDF algorithm (Backward Differentiation Formula), which is an implicit solver that uses backward differentiation formulas with order of accuracy varying from one (also known as the backward Euler method) to five. Furthermore, the solvers termination technique was based on the absolute tolerance (0.0001) for the calculated depending variables (solution). In addition, a mesh sensitivity study was conducted in order to ensure solution convergence. First, a coarse triangular mesh of 5 mm element size was used, where the relative solution is stored. Then the mesh is gradually refined as the new solution still differs from the previous one. Finally, at 0.5 mm element size the solution is converged and the results didn't change as the element size is further decreased. Whereas, the corresponding skewness and condition number mesh characteristics have a minimum element quality above 0.6 and an average element quality of 0.9 for 40000 triangular elements.

Simulation was done in two ways; the first way is by direct implementation of the experimental recorded power $\dot{q}_{exp}(t)$ to COMSOL. On the other hand, the second way is by modelling a controller at the wall temperature (T_2) to imitate the operation of the real controller. For the sake of comparison and validation, relative error between experimental and simulated results, concerning temperatures and energy balance, are calculated using equations (1) and (2) respectively

$$err_{Temp} = \frac{T_{exp} - T_{sim}}{T_{exp} - T_0} * 100 \qquad (1)$$

where T_0 is the initial temperature, T_{exp} is the recorded experimental temperature for a specific spot of the reactor (T_1 till T_5) and T_{sim} is the simulated temperature corresponding to the same position.

$$err_{Energy} = \frac{E_{exp} - E_{sim}}{E_{exp}} * 100 \quad (2)$$

where E_{exp} is the energy consumed by reactor (recorded during experiments) over time by the heaters and E_{sim} is the calculated energy released by the simulated heat source over the same period of time.

3. Mathematical model

After establishing the geometry of the reactor in COMSOL Multiphysics Software, the average thermophysical properties for the reactor and other materials (sand, oil, and PP), shown in Table 2, are defined and applied to the specific partitions of the geometry. Moreover, governing equations, phase change model, and boundary conditions are embedded to model the whole process.

Table 2
Average thermophysical properties in the range of 25-500°C

Materials	Thermal conductivity k (W/(K.m))	Specific heat capacity C_p (J/(kg.K))	Density ρ (kg/m^3)
Stainless steel 321 [24]	16	500	8000
Ceramic fiber [25]	0.12	1000	150
Fine dry Sand [26]	0.2	800	1600
Sunflower oil [27]	0.165	2400	915
Solid PP [10,28]	0.15	1900	900
Molten PP [10,28]	0.16	2200	890

3.1. Governing equations

For the heating process, heat conduction equation, represented by Eq. (3), is used to model heat transfer within the reactor and the loaded material, solid or resting fluid, since there is no fluid flow.

$$\rho C_p \frac{\partial T}{\partial t} = Q + \vec{\nabla} . k\vec{\nabla}T \tag{3}$$

where ρ is the density (kg/m^3), C_p is the specific heat capacity (J/(kg.K)), Q is the volumetric heat source or sink term (W/m^3), $\vec{\nabla}$ is the gradient operator, k is the thermal conductivity (W/(K.m)), and T is temperature (°C). This equation is also used to model heat transfer within molten plastic because of its high viscosity.

In the experiments, a wattmeter is measuring the electrical power (within 1 s time interval) consumed by the heaters, fluctuating with respect to time. This experimental power is implemented as a heat source domain in the present work to mimic the experimental electrical heaters. The time step is adjusted and reduced to be 0.2 s for accuracy.

For fluid flow, energy equation, Eq. (4), is coupled with the momentum equation, Eq. (5), to model heat transfer within a fluid.

$$\rho C_p \frac{\partial T}{\partial t} + \rho C_p \vec{\mathbf{v}} . \vec{\nabla}T = Q + \vec{\nabla} . k\vec{\nabla}T \tag{4}$$

$$\rho \frac{\partial \vec{\mathbf{v}}}{\partial t} + \rho \left(\vec{\mathbf{v}} . \vec{\nabla}\right) \vec{\mathbf{v}} = -\vec{\nabla}p + 2\nabla . (\mu \boldsymbol{S}_{ij}) + \rho\vec{\boldsymbol{F}}_b \tag{5}$$

$$\boldsymbol{S}_{ij} = \frac{1}{2}\left(\nabla \mathbf{v}_{ij} + \nabla \mathbf{v}_{ij}^{\mathrm{T}}\right) \tag{6}$$

where $\vec{\mathbf{v}} = u\vec{\boldsymbol{\imath}} + v\vec{\boldsymbol{\jmath}} + w\vec{\boldsymbol{k}}$ is the velocity vector (m/s), p is the pressure (Pa); μ is the dynamic viscosity (Pa.s); $\boldsymbol{S}_{ij}$ is the strain rate tensor represented by Eq. (6), and $\rho\vec{\boldsymbol{F}}_b$ is the body force acting on fluid. The gravitational force is the body force that interacts with the variation of density due temperature gradient to produce natural flow inside the fluid. This natural fluid motion is modelled using Boussinesq's approximation, which assumes that the density is constant anywhere unless it is multiplied by gravitational field. Therefore, the body force is written as presented in Eq. (7)

$$\rho\vec{\boldsymbol{F}}_b = \rho_{ref}\left(1 - \beta\left(T - T_{ref}\right)\right)\vec{\boldsymbol{g}} \tag{7}$$

where ρ_{ref} and T_{ref} are the reference density and temperature respectively. β is the thermal expansion coefficient (1/K).

3.2. Phase change model

Apparent heat capacity method (AHCM), a built-in feature in COMSOL Multiphysics, was used to model ice and PP melting. This method changes the value of specific heat capacity gradually during a phase change. Moreover, rather than including the latent heat H_L (J/kg) in the energy balance equation at the material phase change temperature T_{pc} ,this heat is distributed within a temperature interval ΔT (transition interval), between $T_{pc} - \Delta T/2$ and $T_{pc} + \Delta T/2$ [29]. Therefore, the heat capacity term, C_p, in Eq. (2) is replaced with a new term called apparent heat capacity, $C_{p,app}$. This new term, described by Eqs. (8) and (9), includes the effective heat capacity, $C_{p,eq}$, of the mixture in the mushy zone (melting range) and the latent heat distribution ($C_L(T)$) over the melting interval. Whereas in this interval (ΔT), there exists a continuous smoothed Heaviside function called θ_1 that models the phase change of the material. This function is equal to 1 before $T_{pc} - \Delta T/2$ and to 0 after $T_{pc} + \Delta T/2$ and it represents the fraction of phase before transition.

$$C_{p,app} = C_{p,eq} + C_L(T) \tag{8}$$

$$C_{p,app} = \frac{1}{\rho_{eq}}\left(\theta_1 \rho_{ph1} C_{p,ph1} + \theta_2 \rho_{ph2} C_{p,ph2}\right) + H_L \frac{d\alpha_m}{dT} \tag{9}$$

where ρ_{eq} is the equivalent density, θ_1 is the phase indicator for phase 1 (*ph1*), $\theta_2 = 1 - \theta_1$ is the phase indicator for phase 2 (*ph2*), ρ_{ph1} is density for phase 1, $C_{p,ph2}$ is specific heat capacity for phase 2, and α_m is the phase mass fraction defined from ρ_{ph1}, ρ_{ph2} and the fraction of phase according to Eq. (10):

$$\alpha_m = \frac{1}{2}\frac{\theta_2 \rho_{ph2} - \theta_1 \rho_{ph1}}{\rho_{eq}} \tag{10}$$

The mass phase fraction is equal to $-1/2$ before transformation and $1/2$ after transformation. Whereas, the equivalent density and thermal conductivity are written in Eq. (11) and Eq. (12):

$$\rho_{eq} = \theta_1 \rho_{ph1} + \theta_2 \rho_{ph2} \tag{11}$$

$$k_{eq} = \theta_1 k_{ph1} + \theta_2 k_{ph2} \tag{12}$$

Madruga et al. [20] led an experimental investigation and a numerical study on tetracosane paraffin within a cubic enclosure. They implemented several K-type thermocouples at different layers in the cube to measure and record the temperature of tetracosane, as it undergoes melting and heating. Moreover, they used the AHCM to model melting process, but instead of using smooth function for phase fraction they used linear function named f_l, described by Eq. (13). Where the derivative of f_l is multiplied with the average density of the material and the latent heat enthalpy for melting (H_L) then added to the energy equation, Eq. (3), as a heat sink (Q) to model the heat absorption as the material undergoes phase changes. Finally, they mentioned that the numerical and experimental results were in a good agreement.

$$f_l = \begin{cases} 0, & T \leq T_s \\ 1, & T \geq T_l \\ (T - T_s)/(T_l - T_s), & T_s < T < T_L \end{cases} \tag{13}$$

T_s (°C) and T_l (°C) are respectively the temperatures of the start and end of the melting process. Moreover, Salvi et al. [23] and Samara et al. [21] also mentioned the apparent heat capacity method in their work. They replaced the specific heat in the energy equation (Eq. (4)) by apparent specific heat ($C_{p,app} = C_{p,avg} + \delta H_L$), where δ, described by Eq. (14) is the Gaussian function used to increase the specific heat smoothly in a small phase change region. But by using this Gaussian function they can't display or modify the phase change function. In addition, simulation may take long time or diverge because of the discontinuity that occurs by the activation of the Gaussian function. In contrast, in the present model the phase change can be displayed for each mesh or point in the domain. Moreover, Murray et al. [22] also used the AHCM to model melting process for octadecane, where they used a simple form for the apparent heat capacity, $C_{p,app} = C_{p,avg} + H_L/\Delta T$.

$$\delta = \frac{exp(-(T - T_{pc})^2/(\Delta T/2)^2)}{(\Delta T/2)\sqrt{\pi}} \tag{14}$$

3.3. Boundary conditions and validation methodology

First, the experimental recorded power $\dot{q}_{exp}$ (W) was implemented into the simulation as a heat source domain Q (W/m^3). In addition, heat loss fluxes due to natural convection q_{conv} (W/m^2), Eq. (15), and radiation q_{rad} (W/m^2), Eq. (16), were applied at the external surface of the insulator. In addition, surface to surface radiation was added between the bottom of the reactor and the insulator to model heat loss due to the air gap at the bottom of the reactor.

$$q_{conv} = h(T_{sur} - T_{amb}) \tag{15}$$

$$q_{rad} = \varepsilon\sigma(T_{sur}^4 - T_{amb}^4) \tag{16}$$

h is the convection heat transfer coefficient (W/(K.m^2)), T_{sur} (°K) is the temperature of the insulator external surface, T_{amb} (K) is the ambient temperature, ε is the surface emissivity, and σ (W/(K^4.m^2)) is the Stefan-Boltzmann constant. The surface emissivity values of stainless steel of reactor walls and insulator's cover are set to $\varepsilon = 0.7$ and, $\varepsilon = 0.4$, respectively [24]. Whereas, the free convection heat transfer coefficient h at the outer wall of the insulator was determined by a built-in empirical correlation for the vertical and horizontal plates [30]. This correlation depends on the *Rayleigh Number* Ra_L, as shown in Eqs. (17-19).

$$Ra_L = Gr_L \,.\, Pr = \frac{g\beta\,(T_{wall} - T_{amb})L^3}{\nu\,.\,\varphi} \tag{17}$$

where Gr_L is the *Grashof Number*, $Pr = \nu/\varphi$ is *Prandtl Number*, $\nu = \mu/\rho$ (m^2/s) is the kinematic viscosity (momentum diffusivity), β is the thermal expansion coefficient (1/K), $\varphi = \rho C_p/k$ (m^2/s) is the thermal diffusivity and L (m) is the characteristic length.

If $Ra_L \leq 10^9$:

$$h = \frac{k}{L}\left(0.68 + \frac{0.67Ra_L^{1/4}}{\left(1 + \left(\frac{0.492k}{\mu C_p}\right)^{9/16}\right)^{4/9}}\right) \tag{18}$$

and if $Ra_L > 10^9$:

$$h = \frac{k}{L}\left(0.825 + \frac{0.387Ra_L^{1/6}}{\left(1 + \left(\frac{0.492k}{\mu C_p}\right)^{9/16}\right)^{8/27}}\right)^2 \tag{19}$$

In addition, the wrapped heating coils around the reactor are not well tight to the reactor wall, so a thin film of air of 0.5 mm thickness is taken between the heating coils and the reactor wall to model the thermal contact between the two surfaces. This reflects a tiny delay or decrease in the temperature and heating rate of the wall. All of these convenient and essential boundary conditions reduce the errors that occur between the experiments and the numerical simulations.

4. Results and discussion

Before modeling the plastic cracking process inside the semi-batch reactor, two steps need to be modeled and validated first; (1) Sensible heat transfer within the reactor's body and feedstock, (2) Plastic melting.

4.1. Modelling and validating empty reactor

First stage of modelling and validating the sensible heat is heating the empty reactor to reach 490 °C at different heating rates (10, 20 and 30 % of the heater full load 1500 W) and comparing the experimental results to the corresponding numerical ones. This step is done to validate the thermal properties and the boundary conditions of the reactor in order to decrease the margin of possible errors that might occur when simulating different phenomena inside the reactor, thus it is a prerequisite step for more complex models. The ranges of the thermal properties as found in literature are as follow: $C_{p,st.\ steel}$ = 490-530 J/K.kg, $k_{st.\ steel}$ = 15-22 W/K.m, $C_{p,insulator}$ = 900-1100 J/K.kg, and $k_{insulator}$ = 0.08-0.16 W/K.m, with respect to temperature range of 25-500 °C [24, 25]. Furthermore, a sensitivity study was performed for the material of the reactor (stainless steel and ceramic fiber insulator) to assess the effects of using temperature dependent thermal properties instead of average values. As a result, it was revealed that only the insulator's thermal conductivity has the major effect on the results, where it increases the average relative error by 3% if the average value was used instead of a temperature dependent value. On the other hand, the effects of using average values for the other properties ($C_{p,st.\ steel}$ = 500 J/K.kg, $k_{st.\ steel}$ = 16 W/K.m, and $C_{p,insulator}$ = 1000 J/K.kg) instead of temperature dependency are neglected, since the average relative error among the two simulated results is less than 1 %. Moreover, it is obvious that their values don't change notably with temperature in contrast to the insulator's thermal conductivity (k_ins) that doubles as temperature increases from 25 to 500 °C.

Moreover, further simplification was taken into consideration by neglecting the natural convection of air inside the reactor and the bottom gap. Whereas, fluid flow simulations were done to emphasize this assumption. The results revealed that less than 1% of change appeared when simulating natural air convection inside the reactor instead of modelling only surface to surface radiation. Therefore, surface to surface radiation was taken as the only mode of heat transfer to reduce the high computational resources required by fluid flow simulation in these regions.

Regarding the results, two types of simulation are realized as referred in section 2.3; (1) Implementing the experimental power $\dot{q}_{exp}(t)$ into simulation as a function of time, and (2) Modelling a controller to mimic the function of the heaters, then comparing the induced

simulated power with the experimental one (err_{Energy}, Eq. (2)). As a result of these two methods, all the temperature relative errors (between simulation and experimental data) among the two methods didn't exceed 2 %, whereas the relative error in energy balance between the induced simulated power and the experimental one didn't exceed 1.5 % when simulating a power controller. Thus, the controller modelling method revealed a good accuracy and aa more realistic way to implement boundary conditions. Furthermore, the results of the two methods are promising as they are compared with the experimental data. Figs. 2-4 show the experimental and simulated results (according to the first method, direct implementation of the experimental power $\dot{q}_{exp}(t)$) for a heating load of 500 W to reach a wall temperature of 490°C followed by a cooling process. in These figures illustrate the four temperatures evolution with respect to time. Modelling was done using Heat Transfer in Solids module in COMSOL Multiphysics software. In addition, PARDISO algorithm was used as a direct solver with the Newton iteration method for numerical simulation.

As shown in Figs. 3 and 4, T_2 (wall) is the controlled temperature located between the heaters on the reactor wall. In addition, the bottom temperature T_3 has almost the same profile as T_2. Moreover, as T_2 approaches 490 °C the regulator undertakes temperature stabilization which leads to periodic fluctuations due to the heater's on and off cycles. It was also noticed that when the heating process ended and the cooling process started at t = 6000 s, the top temperature (T4_exp) remained increasing for a short period of time (from 6000 to 7500 s), in contrast to the simulated temperature T4_sim, which started directly decreasing in a slow cooling rate. Moreover, the cooling rate of T4_exp from 7500 to 10000 s is a bit lower than that of the simulated temperature T4_sim. This difference is due to two effects, first the imperfection of the reactor's insulator, where thermal conductivity decreases between the reactor and the insulator due to the presence of a small air gaps. Secondly, the insulator is taken as a rigid body in the simulation, whereas in reality it is composed of concentric bundles of ceramic fiber blankets . Thus, the heat dissipation from the reactor to the insulator in the simulated model is almost higher than that in reality.

The experimental and simulated results are in good agreement for the four temperatures at different positions with an average relative error lower than 6%. In addition, results of experiments at lower heating rates (heating using 150 and 300 W heating power) revealed the same relative error between the experimental and simulated results.

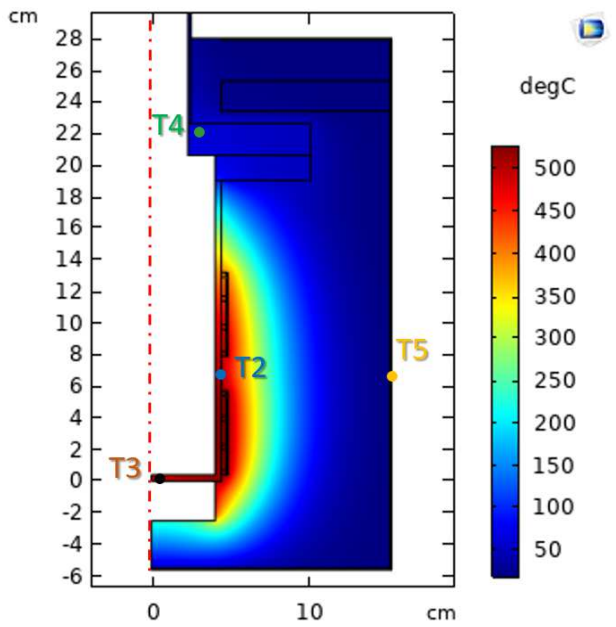

Fig. 2. 2D-axisymmetry simulation for the empty reactor heated using 500 W load, at t = 3000 s.

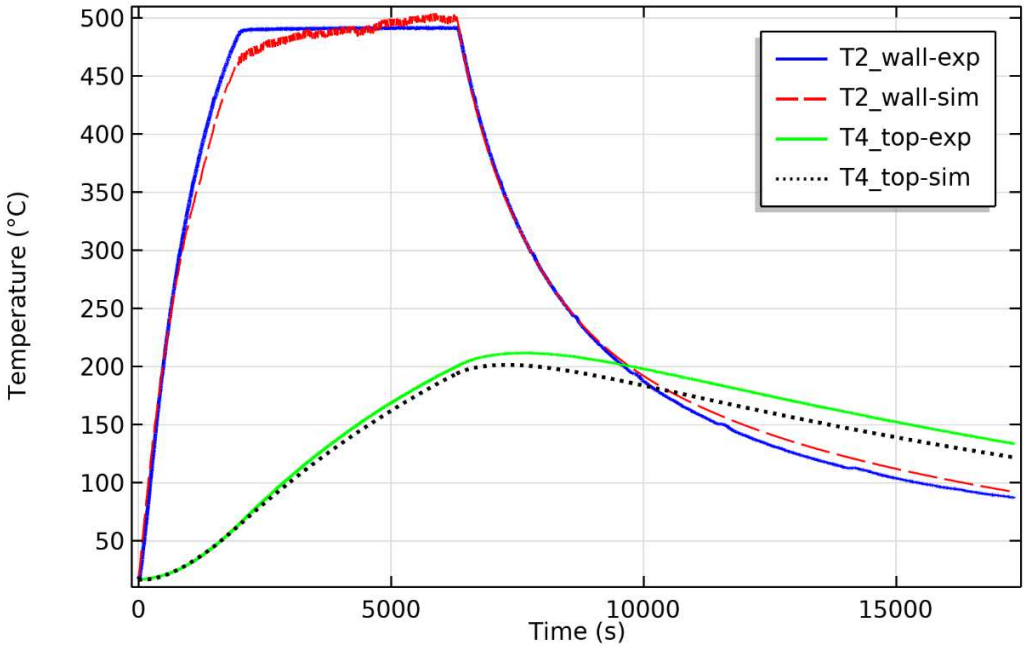

Fig. 3. Temperature comparison, T_{2_wall} and T_{4_top}, for empty reactor heated at 500 W load, T_2 regulated at 490°C.

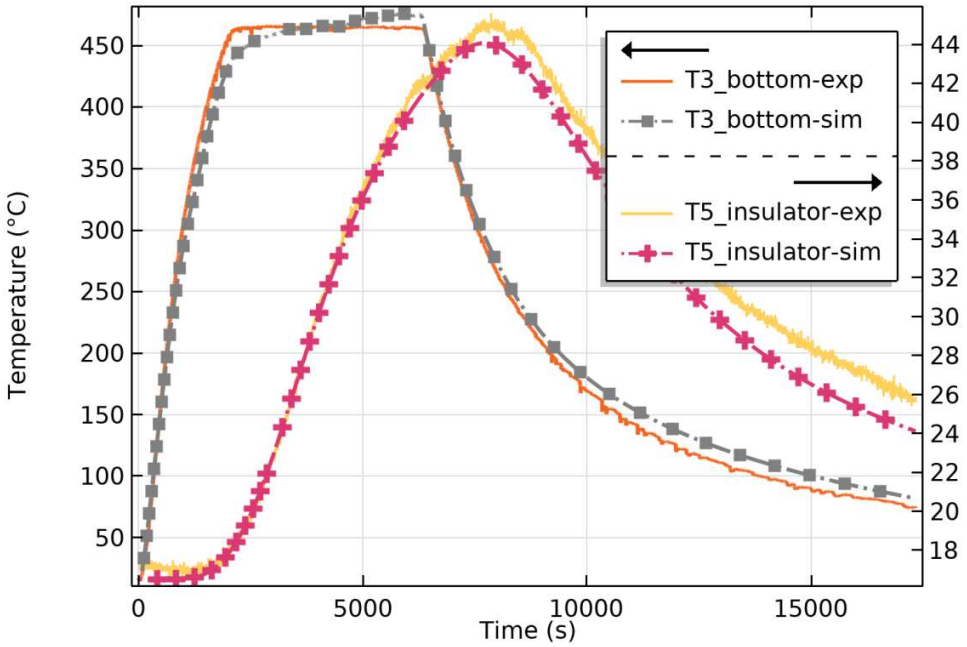

Fig. 4. Temperature comparison, T_{3_bottom} and $T_{5\_insulator}$ for empty reactor heated at 500 W load, T_2 regulated at 490°C..

Furthermore, figs. 5 and 6 show the parity plots for the simulated results and the experimental data for further validation, where the maximum relative error didn't exceed 10 %. Moreover, after validating sensible heat transfer within the empty reactor by using a simulated controller, the reactor is now validated and can be used for any theoretical heating by adjusting the simulated controller temperature. Therefore, the next step is to model and validate heating for different materials inside reactor to upgrade the model and include heating for various materials (solid or fluid).

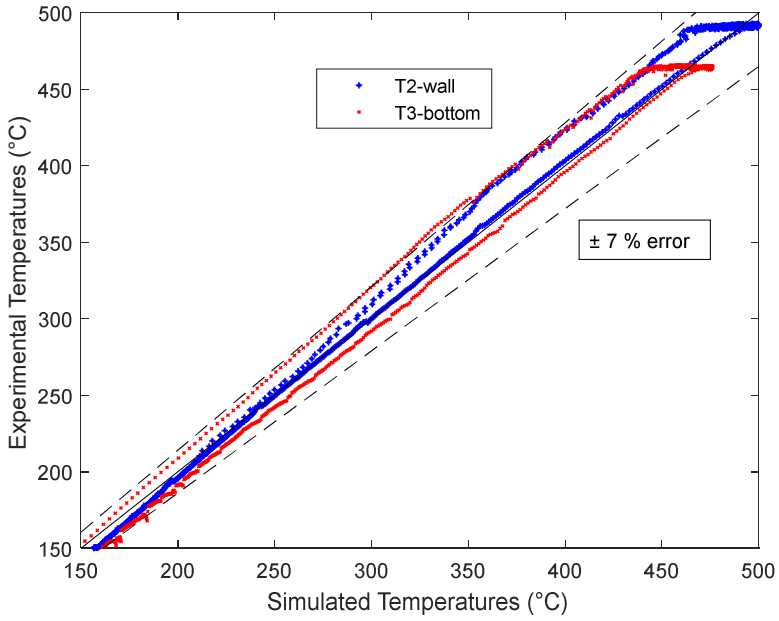

Fig. 5. Parity plot for T_{2_wall} and T_{3_bottom} for empty reactor experiment, heated using 500 W heating load.

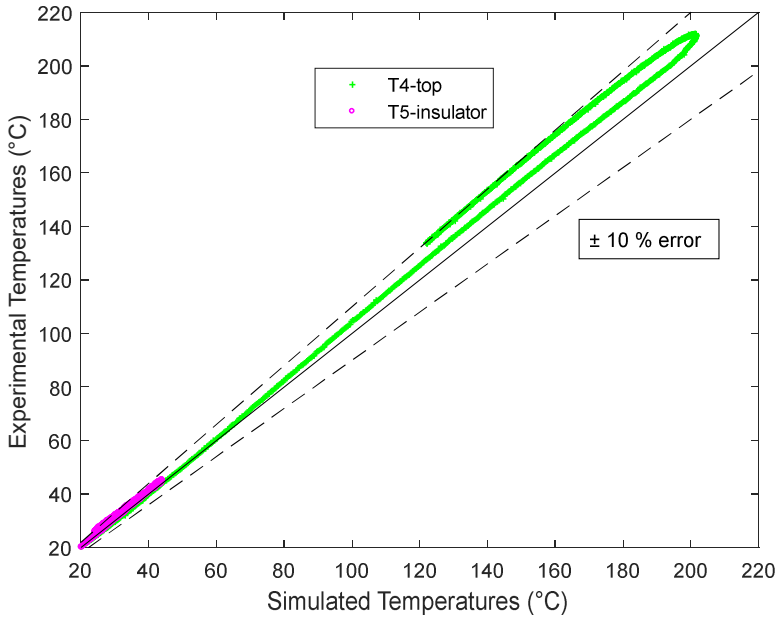

Fig. 6. Parity plot for T_{4_top} and $T_{5\_insulator}$ for empty reactor experiment, , heated using 500 W heating load.

4.2. Modelling and validating sensible heat in a loaded reactor

Now after validating the governing equations, boundary conditions, geometry, simulation settings (mesh size, tolerance, solver, and time step) and material properties, the next step is to check this model when the reactor is loaded.

4.2.1. Heating sand inside the reactor

First, the reactor was filled with fine dry sand particles, and heated to 570°C, then stabilized at this temperature to reach steady state. The loaded sand was modelled as a bulk solid with a measured apparent density of 1484 kg/m^3.

Same as the previous experiments, simulations were done by the two methods. Both methods gave almost the same promising results with 4.5% as an average error in energy balance and 3% as a maximum error among temperatures. But to prevent repetition, only the second method results were presented below in Figs. 7-10, where the heaters are adjusted to 500 W. Fig. 8 shows the controlled temperature T_2 that started fluctuating when it reached 570 °C and then aligned with the experimental results under the regulator's effect. In contrast to Fig. 3, where T_2 started fluctuation before it reached the set point temperature of 490 °C, since heat flux is imposed in simulation (experimental data). The temperature of the top side of the reactor, described by T_4, increases slowly with time due to its position from the heaters and reached almost 280 °C at steady state with an average error of 4% with respect to experiment. Fig. 9 shows the temperature of the bottom of the reactor, $T_{3\_bottom\text{-}sim}$, where it has the same profile as $T_{3\_bottom\text{-}exp}$ with an average relative error of 5%. Regarding Fig. 10, it illustrates the experimental and simulated temperature profiles for the sand inside the reactor, T_1, and the outer wall of the insulator, T_5. The sand temperature (T_1) exceeds the wall temperature (T_2) to reach almost 580 °C because the bottom part of the reactor is hotter than the upper part due to the low inertia (less mass). In addition, thermocouple T_1 is facing the direct heat flux released by the heaters whereas T_2 is located between the two heaters, as shown previously in Fig. 1. Moreover, T_5 reached 50 °C at steady state and the simulated results revealed compatibility with the experimental ones as shown in Fig. 10 with an average relative error less than 4.2 and 5.2% for the sand and insulator temperatures, respectively. Whereas, the average relative error on energy balance, err_{Energy}, is less than 5%. Furthermore, supplementary experiments and simulations conducted at lower heating rates (150 and 300 W heater power) gave the same accuracy, about 5% of average error among temperature and energy balance. Therefore, the model is successfully validated as heating process for reactor loaded with solid material at different temperatures and heating rates. So far, the model can predict the heat distribution with respect to time for any solid material heated inside the reactor with imposed heating power and set point temperature, if the thermal properties of this material are well defined. The next step is to upgrade the model to accept heating fluid materials by validating heating process for a viscous fluid inside the reactor.

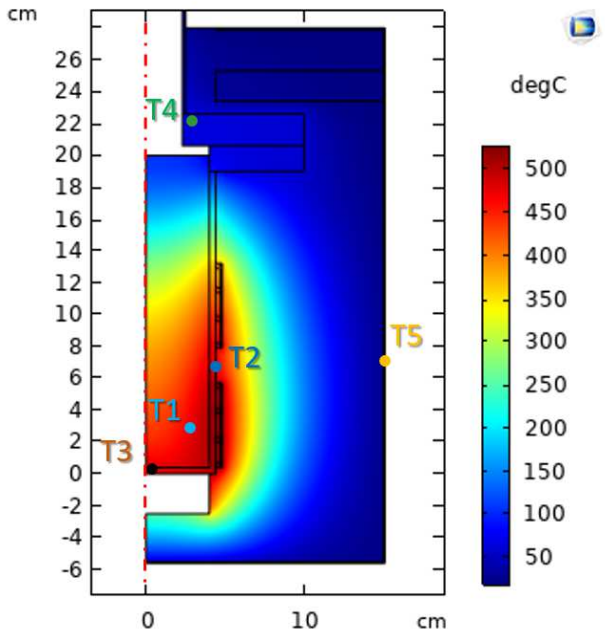

Fig. 7. 2D-axisymmetry simulation for the reactor filled with sand, heated using 500 W load, at t = 6000 s..

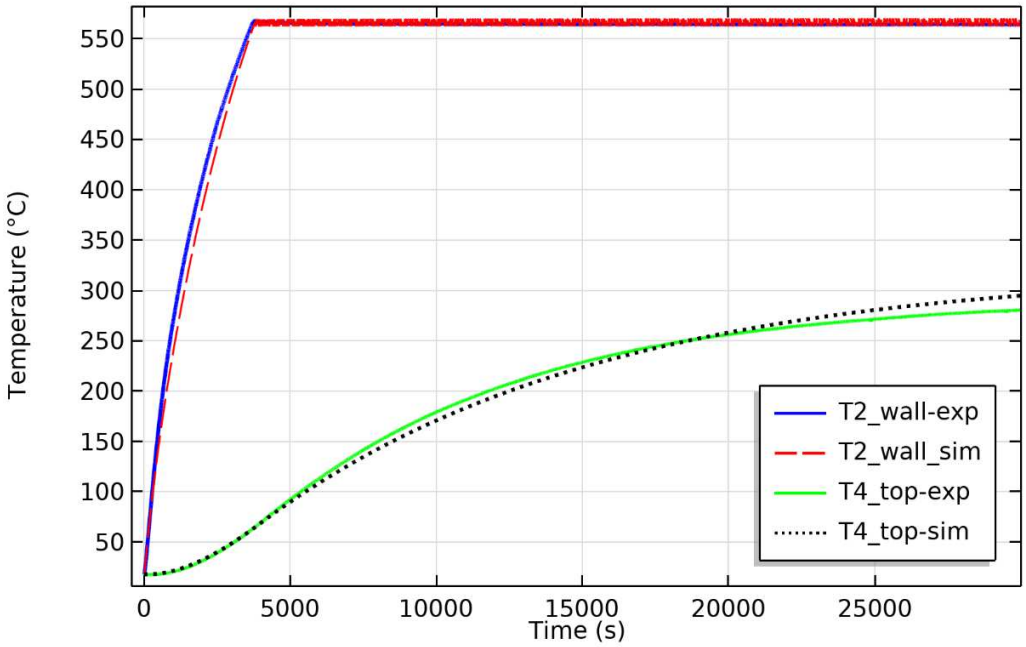

Fig. 8. Temperature comparison, T_2 and T_4, for reactor filled with sand, heated using 500 W load with regulation.

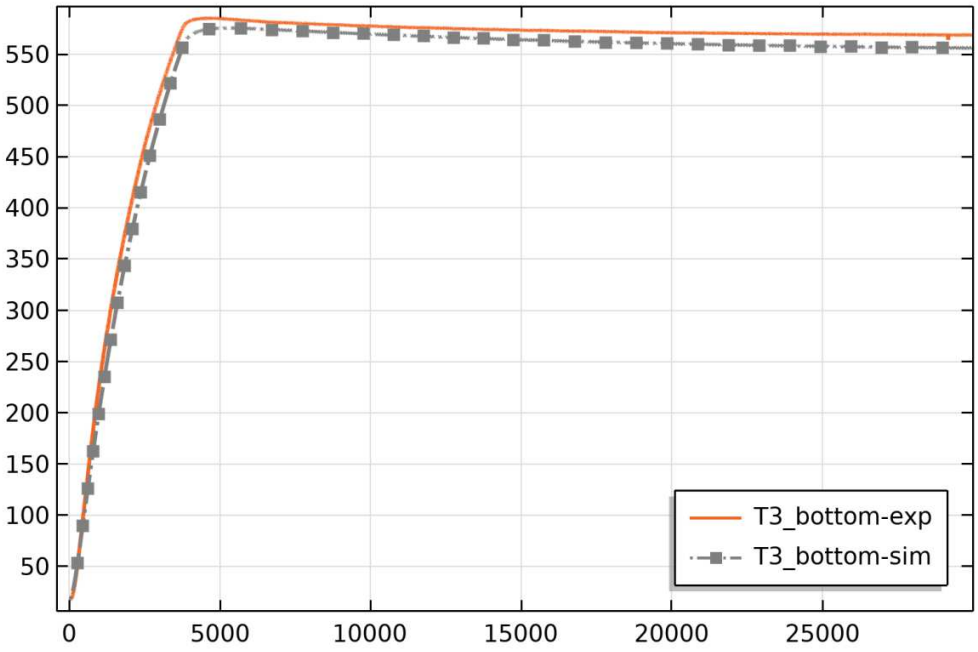

Fig. 9. Temperature comparison, T_{3_bottom}, for reactor filled with sand, heated using 500 W load with regulation.

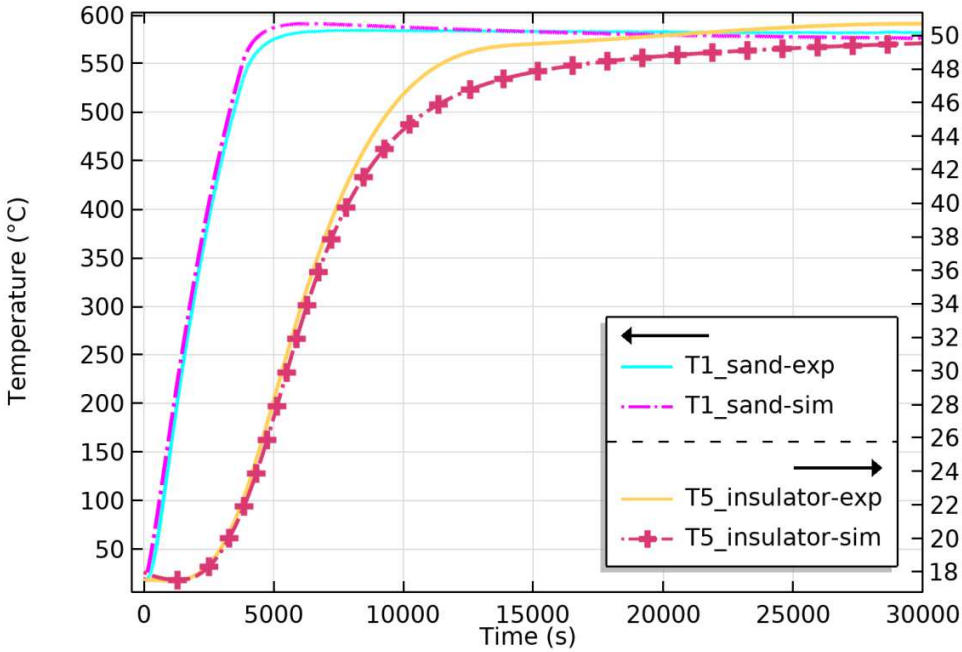

Fig. 10. Temperature comparison, T_{1_sand} and $T_{5\_insulator}$, for reactor filled with sand , heated using 500 W load, with regulation.

4.2.2. Heating sunflower oil inside the reactor

The third stage of modelling and validating sensible heat is heating the reactor with viscous fluid inside. For this sake, the reactor is filled with sunflower oil and heated at different heating rates. In the following experiment, the loaded reactor is heated (500 W) to reach 180 °C and fixed at this temperature for more than one hour. Heat transfer in fluid is modelled by coupling the energy and momentum equations, Eqs. (4) and (5) and by introducing the buoyancy force term, Eq. (7), to conduct the natural fluid flow. Normally, a fluid at atmospheric pressure having a temperature gradient will also demonstrate density gradient within . This slight change in density results in moving downwards the denser fluid that replaces the lighter one. Moreover, this fluid motion enhances heat transfer from the heat source to the fluid's bulk, where this phenomenon is called natural heat convection. In the present model a body force $\rho\vec{F}_b$ called buoyancy force is included (Eq. (7)) in order to take this phenomena in consideration. , According to Boussinesq's approximation, the buoyancy force is proportional to the difference between the local temperature of a fluid zone and the fluid bulk mean temperature (and the thermal expansion property of the material. Therefore, as the fluid near the wall is heated, a body force is activated to move the thin film upwards along the wall and consequently to descend again, which forms an anticlockwise weak fluid vortex shown in Fig 11. This phenomena decays in regions far from the wall where the exerted body force is almost zero, due to low temperature gradient. Furthermore, as time and heat convection proceed, the fluid flow vortex transforms into multiple vortices due to the temperature gradient in the wall itself, as shown in Fig. 12. In addition, the viscosity of the material played an important role in the fluid flow, where it opposed the fluid motion at the beginning of the heating process, where the viscosity was much higher. On the other hand, as the temperature of the fluid is increased with time, the oil viscosity is well decreased too. Thus the fluid could flow more easily and the velocity profiles are increased as have been illustrated in Figs 11 and 12, where the average fluid temperatures are 60 °C and 175 °C respectively. Moreover, the fluid flow is said to be laminar flow because of the low velocity magnitudes.

Simulated results are compared to experimental results for further validation; Three main temperature profiles (T_1, T_2, and T_4), are shown in Fig. 13 and compared with the experimental results. Temperature simulated curves fit well the experimental curves with an average error of 5%, where the energy balance relative error is around 5%. Finally, the presented results prove that the sensible heat transfer within the reactor, empty or loaded (solid or fluid), is modelled and validated at different heating rates. In addition, the model can be used to conduct simulation studies for heating different solid or fluid materials with acceptable results.

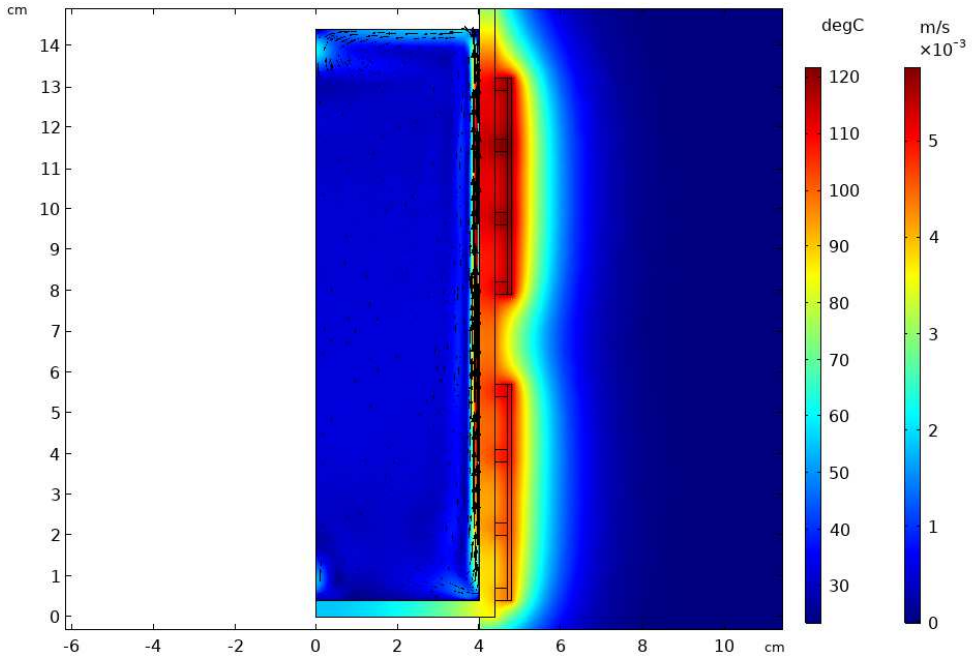

Fig. 11. Surface velocity and temperature profiles for the reactor filled with oil, 500 W, at t = 350 s.

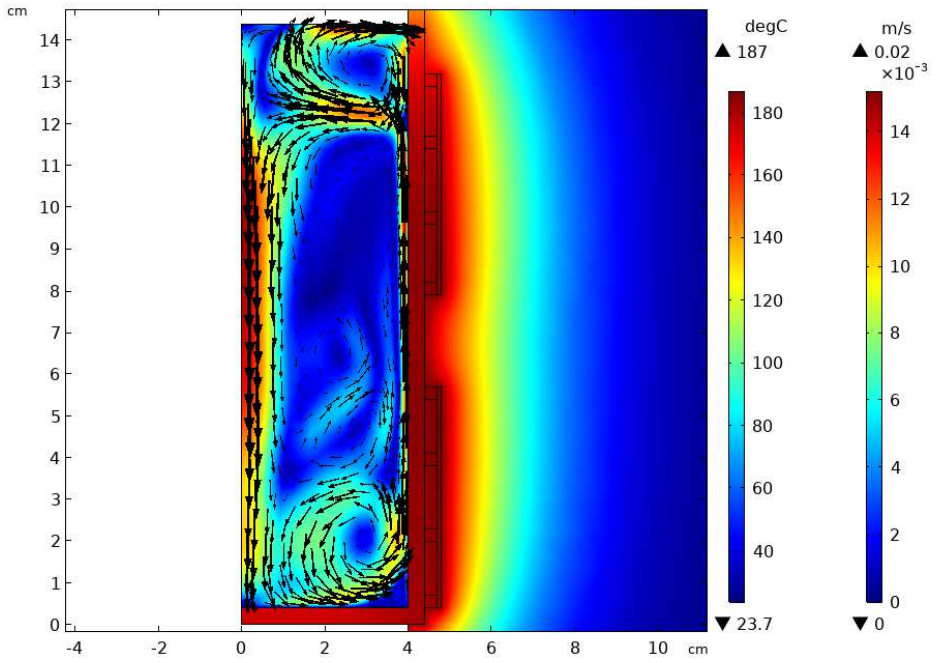

Fig. 12. Surface velocity and temperature profiles for the reactor filled with oil, 500 W, at t = 1700 s.

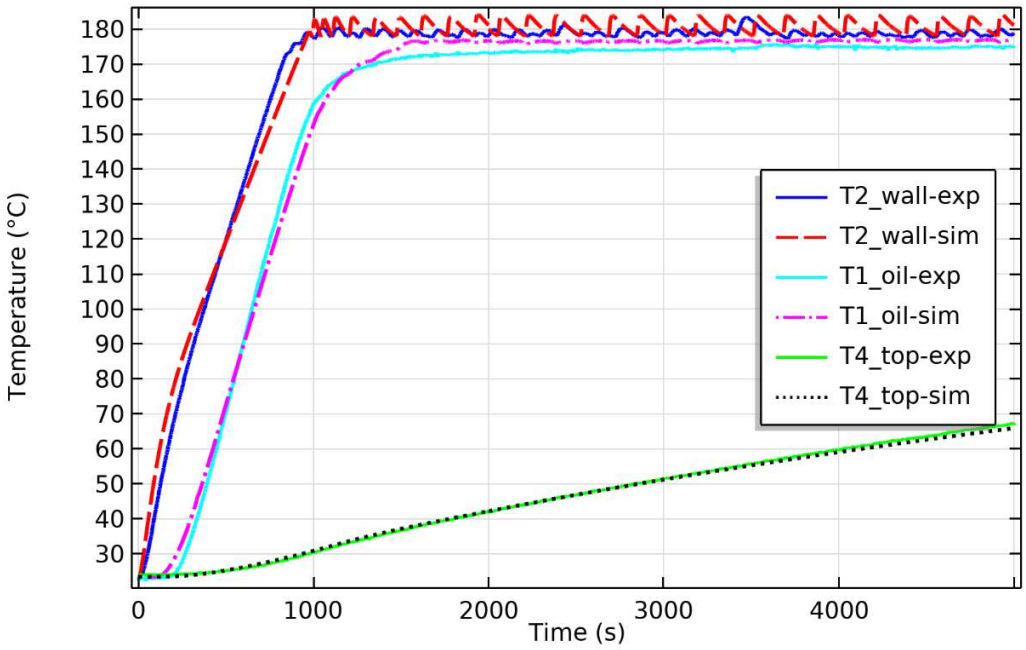

Fig. 13. Temperature comparison, T_{1_oil}, T_{2_wall}, and T_{4_top}, for reactor filled with oil, heated using 500 W.

4.3. Modelling and validating plastic phase change

Prior to modelling plastics melting, the AHCM model is checked validated for ice melting inside the reactor, as a simple experiment using a well-known material and without using heaters.

The reactor is filled and well packed with ice, then, it is let to melt at ambient temperature (T_{amb}=19 °C) without heating. Fig. 14 shows temperature comparison between the simulated and measured temperatures of two thermocouples T_1 and T_4, and as it is obvious from the figure, ice temperature clearly remained constant at the freezing temperature (about 1 °C) before it started rising up when the melting began. This shift in the freezing temperature (from 0 to 1 °C) can be due to the presence of additives from the ice machine, reading errors by the thermocouple and the thickness of the steel cover protecting the thermocouple. The experimental and simulated results show a good agreement with 6% as an average error. Thus, the AHCM revealed a great capability in modelling melting phase.

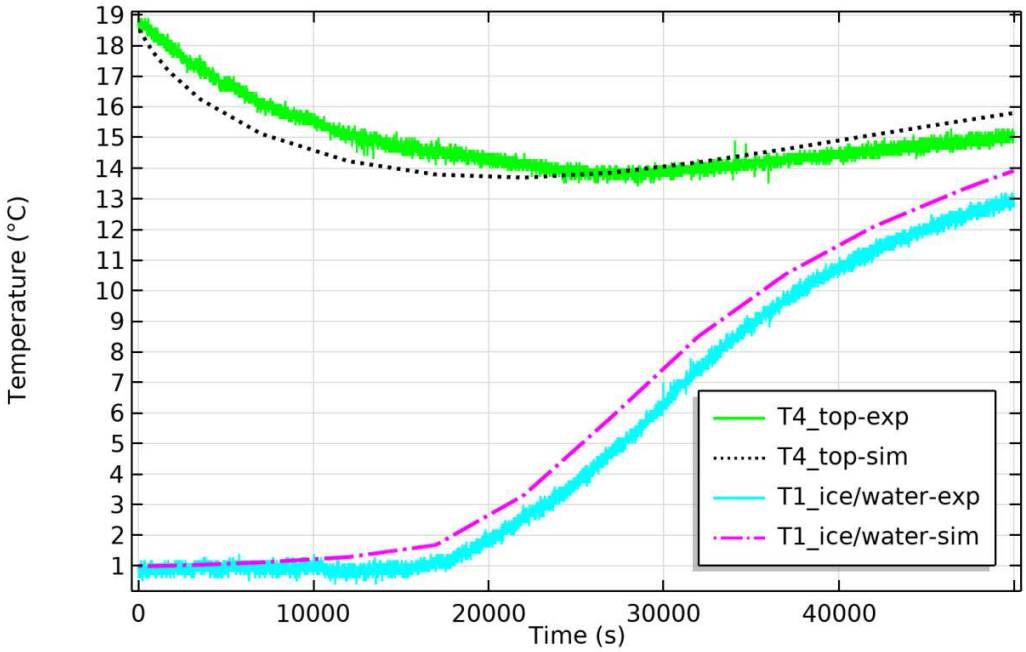

Fig. 14. Temperature comparison, $T_{1\_ice/water}$ and T_{4_top}, ice melting inside the reactor.

In brief, after checking the validity of the AHCM method for melting and the validation of the reactor in heating solid and fluid materials, it can be used now to simulate plastic melting inside the reactor. First, the reactor is prepared with a bulk solid of PP before the experiment is started, as mentioned in part 2. Secondly, loaded plastic is heated to reach 190 °C and then cooled down as shown in Fig. 15 below. The results show that PP temperature (T1) increases linearly by 4.5 °C/min while plastic is in the solid state. Then, it starts bending from the beginning of melting, in the vicinity of 120 °C, till the end (at 170 °C) by a heating rate of 1.33 °C/min. Moreover, the heating rate decreased until reaching a constant value of 0.5 °C/min after melting process, where T_1 reached 185 °C. In contrast to melting, PP temperature remained constant when solidification occurred due to the slow cooling rate in the cooling process, which is less than 1 K/min. Nevertheless, simulated and experimental results have the same tendency and behavior during melting and solidification processes. In addition, the average error obtained from the results is less than 7%. Moreover, Figs. 16 and 17 show the parity plots for the simulated results and the experimental data for further validation, where the maximum relative error didn't exceed 10 %.

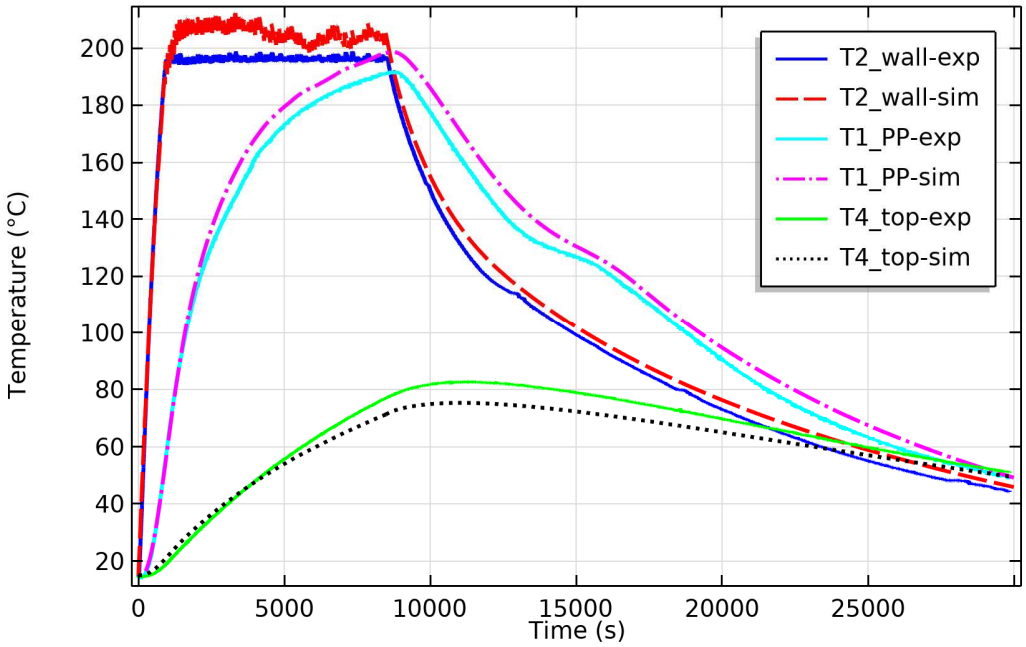

Fig. 15. Temperature comparison, T_{1_PP}, T_{2_wall}, and T_{4_top}, for melting and cooling PP, heated using 500 W load, set point 190°C.

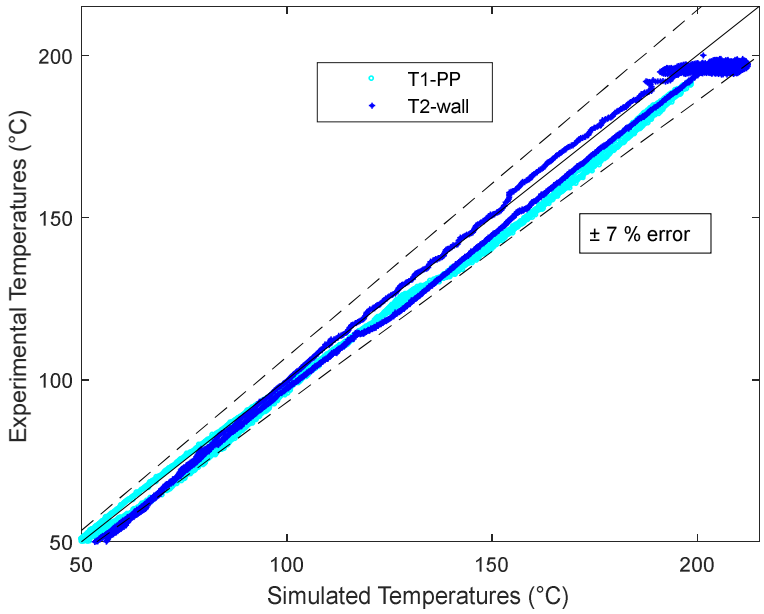

Fig. 16. Parity plot for T_{1_PP}, T_{2_wall}, for melting and cooling PP, heated using 500 W load, set point 190°C.

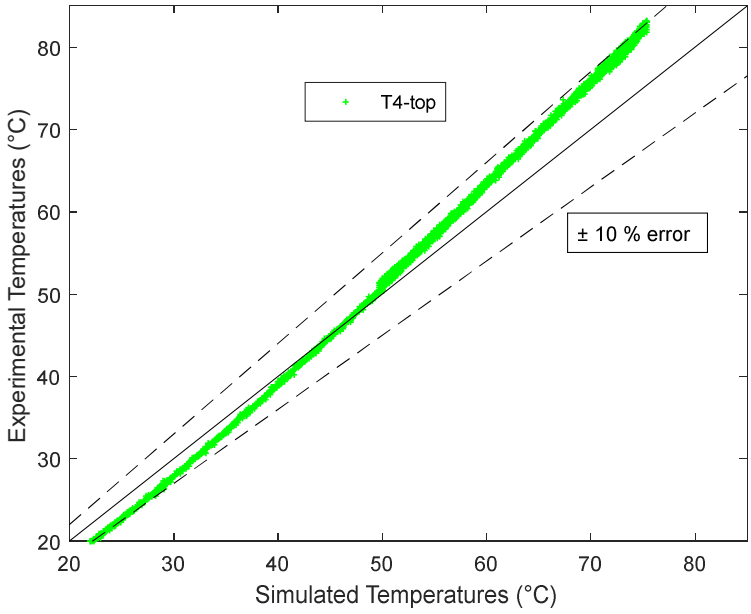

Fig. 17. Parity plot for T_{4_top}, for melting and cooling PP, heated using 500 W load, set point 190°C.

An additional experiment is illustrated below, where PP is melted and heated to reach about 330 °C, which is 60°C lower than the minimum onset temperature, determined by TGA technique. But first, it is good to mention that molten plastic is considered as a bulk of fluid at rest because of its high viscosity, especially at low shear rates (more than 1000 Pa.s) [31]. Thus, there is no fluid flow or motion, which means that only conduction describes heat transfer within the fluid. Fig. 18 presents the results for melting and heating PP to reach 330 °C. It is noticed that, PP temperature curve doesn't obviously bend in the melting range 120-170 °C as it did in the previous experiment; this is due to the higher heating rate which is about 6.4 °C/min. Recalling Fig. 15, plastic started melting when the wall temperature (T_2) was stabilized at 190 °C. On the other hand, in Fig. 18 melting started when the wall temperature was 340 °C. Therefore, the heating rate in the second experiment is much higher than the first, which leads to the little deflection in the curve during melting.

Moreover, T_1 curve is bended again starting from a higher temperature, about 200 °C. The cause of this shift in bending is related to the slow diffusion of heat towards the center. Meanwhile, the simulation results also agree with the experimental data, where the average error is less than 6%. Therefore, it can be said that modelling plastic melting and heating inside the reactor is validated with the experimental results. Also the AHCM revealed a great capability in modelling the melting process for plastic. In addition, the model works well even at relatively high temperatures and heating rates with respect to those found in literature [18-20]. Moreover, the validated heating and melting models can be set as a prerequisite to model plastic cracking Finally, a summary for the relative errors corresponding to the preceding experiments are

displayed in Table 3 below; the maximum average relative error among temperatures in all of the experiments didn't exceed 8%.

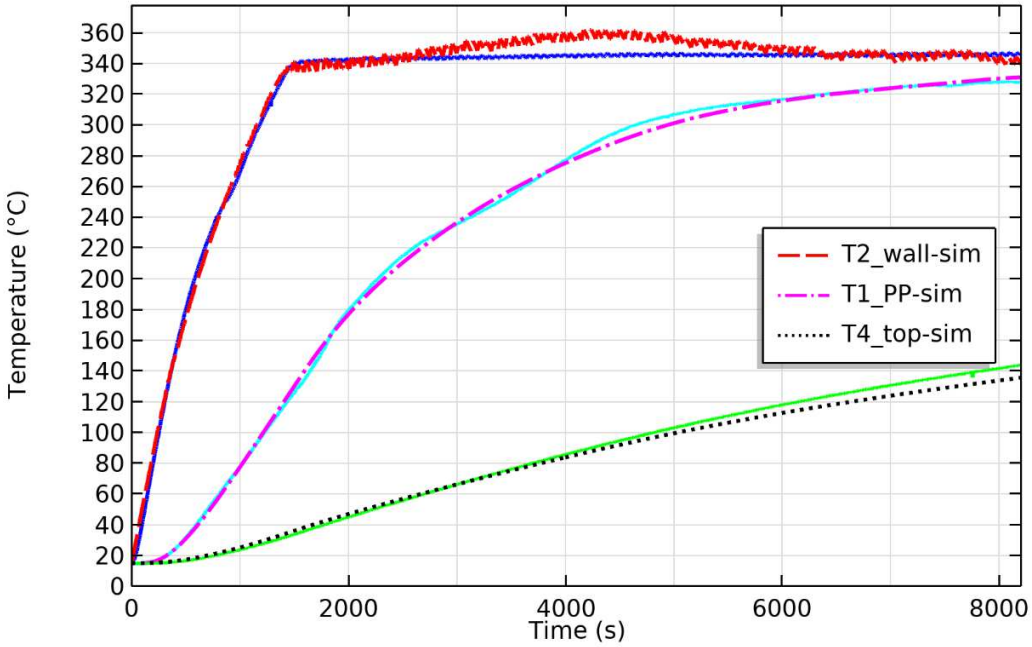

Fig. 19. Temperature comparison, T_1, T_2, and T_4, for melting and heating PP.

Table 3
Temperature and energy relative errors for each experiment.

		Relative error (%)					
Reactor status	**Controller**	**T_1**	**T_2**	**T_3**	**T_4**	**T_5**	**E**
Empty reactor	without Cont.	-	4	4.6	5.8	5.5	-
	with Cont.	-	-	3	7.8	6.5	1.5
Sand heating	without Cont.	4.2	5.5	2	3	5.2	-
	with Cont.	1	-	5	5	5.5	4.5

Oil heating	without Cont.	4.5	3.5	5.8	4	5.5	-
	with Cont.	3.9	-	4.8	3	5	5
Ice melting	without Cont.	6	7	5	6	2	-
PP melting	without Cont.	3	4	3	7	5	-
	with Cont.	4	-	2.5	8	4.5	3.8

It is noteworthy that the outcomes of this work can be useful for different applied energy engineering fields like heat storage using sensible and latent heat, building thermal design for dynamic simulation and modelling the effects of construction material and insulation properties on the thermal performance of the building. The models and assumptions used in this work can also be applied in waste/biomass to energy processes like the simulation of heat transfer process inside pyrolysis reactors (fixed and fluidized beds) or in anaerobic digesters. Also the possibility of using unsteady heat fluxes as boundary conditions can be applied in thermal solar energy application where the intermittence and the fluctuating character of irradiations require dynamic modelling. Finally, the outcomes of simulating oil natural convection inside reactor can be applied to natural convection problems (inside closed cavities or near to vertical walls for example) associated to unsteady temperature/heat flux profiles. Furthermore, the simulation of polypropylene heating and melting process can find application in plastics processing industry like molding and injection in order to enhance exchangers geometries or operating conditions.

5. Conclusions

Plastic pyrolysis is one of the most efficient recovery processes. It converts plastic wastes into liquid and gaseous hydrocarbons under the effect of heating in an inert atmosphere. Plastic pyrolysis includes different sub-processes like heating, melting and cracking. Therefore, the objective of this work is to model processes preceding the cracking of plastic in a semi-batch pyrolysis reactor using finite element method. The work is divided into two stages: (1) Modelling and validating sensible heat transfer in the semi-batch reactor (blank, loaded with sand and oil), (2) Modelling and validating phase change (melting ice and plastic).

An intensive experimental campaign is conducted to apprehend the sensible heat transfer within an empty and loaded semi-batch reactor. Experiments are repeated and recorded at different heating rates. Numerical modelling for each corresponding experiment is achieved and simulation is done using COMSOL Multiphysics software. In addition, sensible heat transfer within the reactor, empty or loaded with solid and liquid materials, is modelled and validated with the experimental results at different heating rates. Moreover, simulation and validation were done for a complex geometry with a significant bulk of materials, heated to elevated temperatures and maintained for long periods of time, which add challenges in setting up the convenient boundary conditions to accurately represent phenomena involved during the process. Also, a simulated controller is modelled to mimic the power input of different experiments.

Apparent heat capacity method was used to model phase change process for ice and polypropylene, which revealed high capability and accuracy in modelling and simulation. Moreover, the enhanced method that is used in the simulation is more convenient and accurate in modelling phase change (melting) than the other methods found in literature. Since this method depends on an adjustable average weighted smoothed conversion function over a phase change temperature interval that can be monitored and illustrated. In addition, molten plastic was modelled as a bulk of fluid at rest, because of its high viscosity. Furthermore, plastic melting/solidification and heating/cooling processes are modelled and validated with the experimental results at different heating rates. The validated models of heating and melting can be set as a prerequisite to simulate the plastic cracking process inside the reactor.

Governing equations, boundary conditions, geometry, simulation settings (mesh size, tolerance, solver, and time step) and material properties described well the reactor and heat transfer within it. The maximum average error obtained in all the simulation is less than 8%. Finally, this validated model is paving the way for modelling pyrolysis process of plastics. In addition, the outcomes of the presented model can be extended to different applied energy engineering fields like waste/biomass to energy, heat storage, building heating and cooling, thermoplastics processing and equipment design and other unsteady heat flux/temperature problems applications.

References

[1] Plastics – the Facts 2019, An analysis of European plastics production; demand and waste data, PlasticEurope, Association of Plastics Manufacturers, (2019).

[2] R. Geyer, J.R. Jambeck, K.L. Law, Production, use, and fate of all plastics ever made, Science Advances 2017;3.

[3] S.D.A. Sharuddin, F. Abnisa, W.M.A.Wan Daud, M.K. Aroua, A review on pyrolysis of plastic wastes, Energy Convers. Manage. 2016;115:308-326.

[4] A. Aboulkas, K. El harfi, A. El Bouadili, Thermal degradation behaviors of polyethylene and polypropylene. Part I: Pyrolysis kinetics and mechanisms, Energy Convers. Manage. 2010;51:1363-1369.

[5] F. Xu, B. Wang, D. Yang, J. Hao, Y. Tian, Thermal degradation of typical plastics under high heating rate conditions by TG-FTIR: Pyrolysis behaviors and kinetic analysis, Energy Convers. Manage. 2018;171:1106-1115.

[6] C. Kassargy, S. Awad, G. Burnens, K. Kahine, M. Tazerout, Experimental study of catalytic pyrolysis of polyethylene and polypropylene over USY zeolite and separation to gasoline and diesel-like fuels, J. Anal. Appl. Pyrolysis 2017;127:31-37.

[7] Y. Zheng, L. Tao, X. Yang, Y. Huang, Z. Zheng, Study of the thermal behavior, kinetics, and product characterization of biomass and low-density polyethylene co-pyrolysis by thermogravimetric analysis and pyrolysis-GC/MS, J. Anal. Appl. Pyrolysis 2018;133:185-197.

[8] H. Bockhorn, A. Hornung, U. Hornung, et al., Modelling of isothermal and dynamic pyrolysis of plastics considering non-homogeneous temperature distribution and detailed degradation mechanism, J. Anal. Appl. Pyrolysis 1999;49:53-74.

[9] M.V. Navarro, J.D. Martínez, R. Murillo, et al., Application of a particle model to pyrolysis. Comparison of different feedstock: Plastic, tyre, coal and biomass, Fuel Process. Technol. 2012;103:1-8.

[10] Z. Jin, L. Yin, D. Chen, Y. Jia, B. Yu, Heat transfer characteristics of molten plastics in a vertical falling film reactor, Chin. J. Chem. Eng. 2019;27:1015-1020.

[11] S. Liu, Y.L. Hao, Numerical simulation on gas–liquid two-phase motion of falling film in vertical tube, J. Therm. Sci. Technol. 2008;7:5-10.

[12] E.G. Puckett, A.S. Almgren, J.B. Bell, et al., A high-order projection method for tracking fluid interfaces in variable density incompressible flows, J. Comput. Phys. 1997;130:269-282.

[13] K. Yan, D.F. Che, A coupled model for simulation of the gas–liquid two-phase flow with complex flow patterns, Int. J. Multiphase Flow 2010;36:333-348.

[14] H. Wang, L.J. Yin, D.Z. Chen, et al., Heat transfer characteristics of MSW and its typical components in rotary kiln at different pyrolysis stages, J. Chem. Ind. Eng. 2014;65:4716-4725.

[15] B. Csukas, M. Varga, N. Miskolczi, S. Balogh, A. Angyal, L. Bartha, Simplified dynamic simulation model of plastic waste pyrolysis in laboratory and pilot scale tubular reactor, Fuel Processing Technology 2013;106:186-200.

[16] K. Ding, Q. Xiong, Z. Zhong, CFD simulation of combustible solid waste pyrolysis in a fluidized bed reactor, Powder Technology 2020;362:177-187.

[17] J.M. Encinara, J.F. González, Pyrolysis of synthetic polymers and plastic wastes. Kinetic study, Fuel Process. Technol. 2008;89:678-686.

[18] Dabiri Atashbeyk M., Shahbazi K., Fattahi M., Pressure Profile Estimation through CFD in UBD Operation Considering with Influx to Wellbore, Iran. J. Chem. Chem. Eng., Vol. 37, No. 6, 2018.

[19] Moradi F., Kazemeini M., Fattahi M., A Three Dimensional CFD Simulation and Optimization of Direct DME Synthesis in a Fixed Bed Reactor, Pet. Sci.,11(2): 323-330 (2014).

[20] S. Madruga, N. Haruki, A. Horibe, Experimental and numerical study of melting of the phase change material tetracosane, International Communication in Heat and Mass Transfer 98 (2018) 163-170.

[21] F. Samara, D. Groulx, and P. H. Biwole, Natural Convection Driven Melting of Phase Change Material: Comparison of Two Methods, COMSOL Conference 2012 Boston.

[22] R. E. Murray and D. Groulx, Modelling Convection during Melting of a Phase Change Material, COMSOL Conference 2011 Boston.

[23] D. Salvi, D. Boldor, G.M. Aita, C.M. Sabliov, COMSOL Multiphysics model for continuous flow microwave heating of liquids, Journal of Food Engineering 104 (2011) 422-429.

[24] Engineering Properties of steels, Philip D. Harvey, American Society for Metals (1982).

[25] Materials for energy efficiency and thermal comfort in buildings Edited by Matthew R. Hall New York Washington, DC, wood head publishing limited (2010).

[26] I.N. Hamdhan, B.G. Clarke, Determination of Thermal Conductivity of Coarse and Fine Sand Soils, Proceedings World Geothermal Congress 2010.

[27] E.E.G. Rojas, J.S.R. Coimbra, J.T. Romero, Thermophysical Properties of Cotton, Canola, Sunflower and Soybean Oils as a Function of Temperature, International Journal of Food Properties 2013;16:1620-1629.

[28] Typical Engineering Properties of Polypropylene, INEOS Olefins and Polymers USA.

[29] Heat Transfer Module User's Guide, COMSOL Multiphysics.

[30] FRANK P. INCROPERA, Fundamentals of Heat and Mass Transfer, SIXTH EDITION, College of Engineering University of Notre Dame (2007).

[31] J. F. Asassant, F. Pigeonneau, L. Sardo, M. Vincent, Flow analysis of the polymer spreading during extrusion additive manufacturing, Additive Manufacturing 2019;29: 100794.